

# A Mucin-Based Bio-Ink for 3D Printing of Objects with Anti-Biofouling Properties

Carolin A. Rickert, Salma Mansi, Di Fan, Petra Mela, and Oliver Lieleg\*

With its potential to revolutionize the field of personalized medicine by producing customized medical devices and constructs for tissue engineering at low costs, 3D printing has emerged as a highly promising technology. Recent advancements have sparked increasing interest in the printing of biopolymeric hydrogels. However, owing to the limited printability of those soft materials, the lack of variability in available bio-inks remains a major challenge. In this study, a novel bio-ink is developed based on functionalized mucin—a glycoprotein that exhibits a multitude of biomedically interesting properties such as immunomodulating activity and strong anti-biofouling behavior. To achieve sufficient printability of the mucin-based ink, its rheological properties are tuned by incorporating Laponite XLG as a stabilizing agent. It is shown that cured objects generated from this novel bio-ink exhibit mechanical properties partially similar to that of soft tissue, show strong anti-biofouling properties, good biocompatibility, tunable cell adhesion, and immunomodulating behavior. The presented findings suggest that this 3D printable bio-ink has a great potential for a wide range of biomedical applications, including tissue engineering, wound healing, and soft robotics.

## 1. Introduction

From rapid prototyping to personalized manufacturing—3D printing (3DP) transforms the way we design and produce objects. 3DP creates the opportunity to fabricate highly complex, multiscale structures with great design flexibility by directly translating virtual 3D models into physical objects. Owing to ongoing improvements of printing processes<sup>[1]</sup> and the growing variety of printable materials,<sup>[2]</sup> 3DP has evolved from a fabrication method mostly used for rapid prototyping to a feasible technique

for the on-demand manufacturing of objects with tailored dimensions and properties.<sup>[3]</sup>

This development has also strongly influenced the field of biomedical engineering.<sup>[4]</sup> Among the multitude of developed additive manufacturing techniques, extrusion-based 3DP methods such as fused deposition modeling of thermoplastics or direct ink writing of photosensitive polymer resins have demonstrated a high potential for the production of customized (bio)medical and surgical devices or scaffolds—based on tomography data or computer aided design.<sup>[5]</sup> In those techniques, the liquid ink, i.e., a viscous polymer solution or a melt—is gently pushed through a nozzle, that follows a predetermined path dictated by a virtual model; during this procedure, the ink is deposited onto a printing bed to build the desired object in a layer-by-layer fashion and from bottom to top.


To be able to precisely create structures in three dimensions without the need for molds or machining, controlling the material properties of the printing material is key.<sup>[6]</sup> Therefore, the ink material must meet different specifications in terms of printability and stability.<sup>[7]</sup> This encompasses the ability to be extruded from a nozzle or printing head (which requires the material to flow when exposed to modest pressure), to be quickly curable upon deposition (e.g., by photopolymerization, thixotropic effects, or temperature changes) and to exhibit mechanical properties that are sufficiently strong to support the following layers.<sup>[8]</sup> Meeting all

C. A. Rickert, D. Fan, O. Lieleg  
TUM School of Engineering and Design  
Department of Materials Engineering  
Technical University of Munich  
Boltzmannstr. 15, 85748 Garching b. München, Germany  
E-mail: oliver.lieleg@tum.de

C. A. Rickert, D. Fan, O. Lieleg  
Center for Functional Protein Assemblies (CPA)  
Technical University of Munich  
Ernst-Otto-Fischer Str. 8, 85748 Garching b. München, Germany

S. Mansi, P. Mela  
TUM School of Engineering and Design  
Department of Mechanical Engineering  
Chair of Medical Materials and Implants  
Technical University of Munich  
Boltzmannstr. 15, 85748 Garching b. München, Germany

S. Mansi, P. Mela  
Munich Institute of Biomedical Engineering and Munich Institute of Integrated Materials  
Energy and Process Engineering  
Technical University of Munich  
Boltzmannstr. 15, 85748 Garching, Germany

 The ORCID identification number(s) for the author(s) of this article can be found under <https://doi.org/10.1002/mabi.202300198>

© 2023 The Authors. Macromolecular Bioscience published by Wiley-VCH GmbH. This is an open access article under the terms of the Creative Commons Attribution-NonCommercial License, which permits use, distribution and reproduction in any medium, provided the original work is properly cited and is not used for commercial purposes.

DOI: 10.1002/mabi.202300198

these requirements can be difficult for newly developed ink materials; in fact, the lack of diversity in 3D printable biomaterials remains a significant challenge in biomedical engineering: Objects intended for different applications usually also require a different set of characteristics, such as certain mechanical properties, the ability for cells to adhere or even colonize the sample, bioactivity, or nutrient permeability. However, many commonly used, commercially available bio-inks have a rather narrow range of characteristics. Hence, to allow for generating objects for a broader spectrum of applications, a more versatile set of bio-ink components with a similarly broader range of properties is required.

In this context, the material class of hydrogel bio-inks has recently gained increased attention for biomedical applications including tissue engineering,<sup>[9]</sup> biomolecule/drug delivery,<sup>[10]</sup> soft robotics,<sup>[11]</sup> or flexible electronics.<sup>[12]</sup> Furthermore, hydrogel bio-inks were recognized as promising candidates for patient-tailored regenerative medicine, which seeks to repair or replace damaged or dysfunctional tissues.<sup>[13]</sup> However, using hydrogels as inks comes with a major challenge: they tend to spread on the surface immediately after deposition and their mechanical properties are comparatively weak—even after curing.<sup>[14]</sup> Those factors limit the achievable resolution of the generated structures: the usually rather low viscosity and strong shear-thinning properties of hydrogels make it difficult to precisely control the ink during the printing process, and this prevents the creation of high-resolution features. In addition, compared to the rapid curing techniques used for plastics, such as heat-induced melting and solidification, the crosslinking methods employed for hydrogel bio-inks, such as photopolymerization or enzymatic crosslinking, often require longer exposure times or incubation periods—and the material must remain intrinsically stable during those crosslinking steps before it reaches its final stability. During those longer curing times, biopolymeric hydrogels, which primarily consist of water, can deform or flow under the influence of gravity alone. To some extent, such an insufficient intrinsic stability of hydrogel bio-inks can even persist after curing of individual layers or fully printed samples; then, printing thin, instable structures might require supporting structures to prevent the printed object from collapsing under its own weight.

Moreover, biopolymeric hydrogels often require additional processing steps beyond the printing process itself. These steps can include postprinting crosslinking or gelation to further stabilize the printed structure. Crosslinking agents or external stimuli such as UV light, temperature, or chemical reactions may be needed to induce gelation or crosslinking of the hydrogel material. These additional steps add complexity to the printing process and increase the overall fabrication time. Furthermore, bio-inks must not only be suited for the fabrication process but also for the intended medical application, e.g., they need to be biocompatible.<sup>[15]</sup> Here, several biopolymers, including alginate,<sup>[16]</sup> hyaluronic acid,<sup>[17]</sup> and gelatin<sup>[18]</sup> have recently been shown to be good candidates as base materials for bio-inks. However, whereas those biopolymers mainly satisfy the mechanical properties required for 3D bioprinting, multifunctional polymers could provide a broader range of biomedically beneficial properties, such as bioactivity or tailored cell adhesion. For example, inks with an intrinsic anti-biofouling behavior would be

desirable: such biofouling—which refers to the unwanted accumulation of, e.g., bacteria, proteins, or cells, on the surface of objects such as medical devices or implants—is a major risk factor in the application of medical devices as it can lead to severe infections.<sup>[19]</sup>

Here, mucins constitute a promising class of biological macromolecules and have recently received increasing attention as multifunctional components of different biomaterials.<sup>[20]</sup> Such mucins are highly glycosylated proteins that play a major role for the inherent immune barrier of mammals: They constitute the macromolecular key component of mucus, the viscoelastic hydrogel that covers all wet epithelia and serves as a first line of defense against pathogenic invaders.<sup>[21]</sup> Those glycoproteins have relatively high molecular weights (several MDa), comprise a long polypeptide backbone including a densely glycosylated, polyanionic and hydrophilic core region and sparsely glycosylated, partially folded, and hydrophobic terminal regions.<sup>[22]</sup> In addition to their role as antiviral and antibacterial agents,<sup>[23]</sup> mucins exhibit several other interesting characteristics such as the ability to bind water,<sup>[24]</sup> to form gels at acidic pH,<sup>[25]</sup> and to act as an excellent lubricant.<sup>[26]</sup> Furthermore, owing to their complex biochemical architecture, mucins provide interaction sites toward both, hydrophobic and hydrophilic (and this includes anionic and cationic) molecules and particles.<sup>[27]</sup> Indeed, purified mucins were recently used as a versatile carrier system for sustained drug release,<sup>[28]</sup> as cell- and bacteria repellent coatings,<sup>[29]</sup> and as a protective layer to prevent tissue damages induced by medical devices.<sup>[30]</sup> For those applications, mucins were mainly used as solutions or as surface coatings on already existing medical devices. However, recent studies also indicate the possible benefits of stable bulk materials generated from mucin molecules.<sup>[31]</sup>

In this study, we introduce a mucin-based bio-ink as a novel material for 3D bio-printing. In detail, functionalized porcine gastric mucins are integrated into a hydrogel generated from Laponite XLG—a layered silicate made from naturally occurring, inorganic mineral sources. We show that this two-component hydrogel system combines the medically beneficial characteristics of mucin molecules with the good printability and short-term stability of the Laponite. Cured objects generated from the developed mucin-based bio-ink exhibit remarkable anti-biofouling properties (i.e., the ability to repel bacteria and cells) and very good biocompatibility. We characterize the mechanical properties of the cured bio-ink and we show that the presence of mucins in the material dampens the immune response of macrophages. With this novel bio-ink, it is now possible to 3D-print mucin-based materials—and this constitutes a fully new processing method for mucin glycoproteins. Thus, our study provides a major stepping stone toward the exploitation of the extraordinary properties of mucin glycoproteins for a broad range of biomedical applications.

## 2. Experimental Section

If not stated otherwise, all chemicals were obtained from Carl Roth GmbH & Co. KG (Karlsruhe, Germany). Double distilled water (ddH<sub>2</sub>O, pH 7.0) was freshly prepared for each experiment.

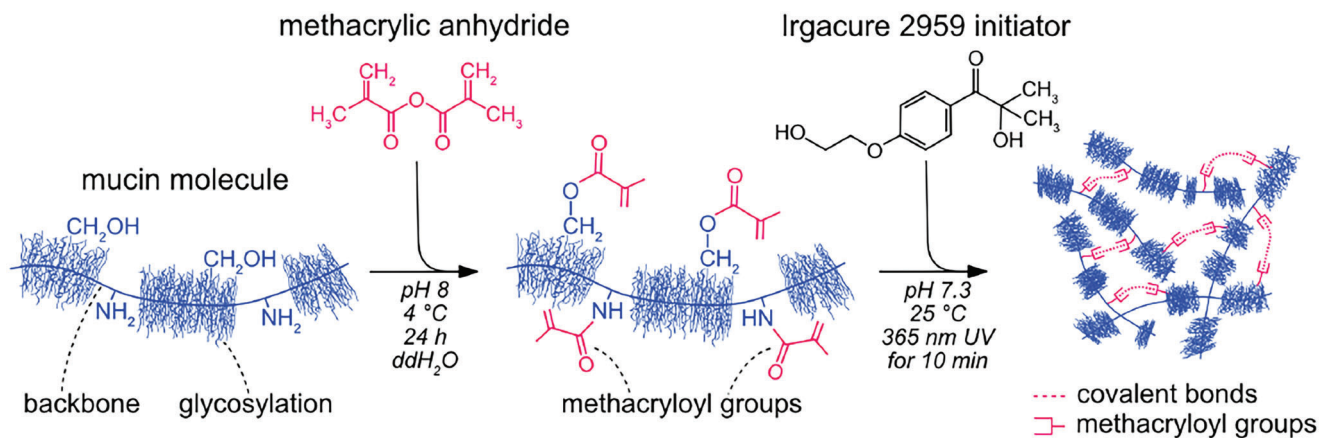


**Figure 1.** Schematic representation of the methacrylation procedure of PGM and the UV-driven curing of PGM-MA. PGM molecules were methacrylated via the hydroxymethyl groups of their glycans and the amine groups of the protein backbone. Crosslinking was achieved by adding the photoinitiator Irgacure 2959 and subsequent UV irradiation.

### 2.1. 3D Printing Process

For 3D printing of the mucin-based materials, a fused deposition modeling bioprinter was used (BioX, Cellink, Göteborg, Sweden). The printer reaches a nominal mechanical resolution of 1  $\mu\text{m}$  for both, horizontal  $x/y$  movements and vertical movements in  $z$  (layer resolution). All printing procedures were performed at room temperature using a needle gauge of 25G. This needle gauge was chosen to ensure good extrudability of the ink despite certain variability of the ink characteristics (see Section 3.5). Here, already small variations in the viscosity could lead to leakage of the ink or over-extrusion (for big needle diameters such as 20G or 22G), or they could induce clogging of the needle (for small needle diameters such as 27G or 30G). If not stated otherwise, an extrusion pressure of 80 kPa was applied and a moving speed of 20  $\text{mm s}^{-1}$  was selected. After inserting the mucin-based ink materials into the UV-protected cartridge (to prevent premature photopolymerization) and attaching the needle, the cartridge was mounted into the printer and a manual calibration was conducted. During the printing process, the printing area was permanently irradiated with UV light (via the integrated 365 nm UV module of the BioX printer) and a 365 nm UV-curing head was used to cure each layer directly after extrusion for 30 s at a distance of 2 cm. In addition, after printing of a complete structure, the sample was irradiated for 5 more minutes to ensure sufficient curing of all printed layers.

### 2.2. Functionalization of Porcine Gastric Mucin with Methacryloyl Groups

To attach photo-crosslinkable groups to porcine gastric mucins (PGM; mucin from porcine stomach Type II; Sigma-Aldrich, St. Louis, MO), PGM was chemically modified with methacrylic anhydride (MA; Sigma-Aldrich; **Figure 1**). Although lab-purified mucin may offer higher purity, here, commercial PGM was favored due to its easier availability and cost-effectiveness. Since the structural losses previously reported for commercial PGM molecules mainly affect the ability of mucins to passively adhere

to surfaces and to undergo gelation at acidic pH,<sup>[32]</sup> we expect those mucins to be sufficiently intact to be used as components of a bio-ink.

The PGM was first dissolved in DMSO (20  $\mu\text{L}$  DMSO per mg mucin) and then diluted with ddH<sub>2</sub>O to reach a final mucin concentration of 1.0 % (w/v). Afterward, the pH was adjusted to  $\approx 8.0$  while cooling the mucin solution on ice. Once cooled down, MA was added to the mucin solution to obtain a final MA to PGM ratio of 1000/1 (i.e., 1000 MA molecules per PGM macromolecule). Within the initial 6 h after mixing, the pH of the solution continuously decreased and was thus repeatedly readjusted to 8.0 by adding 5 M NaOH while gently stirring the solution. Subsequently, the solution was stored at 4 °C overnight to allow for further reaction. To remove nonreacted MA and mucin precipitations, a centrifugation step (10 min, 5000 rpm, Centrifuge 5430, Eppendorf SE, Hamburg, Germany) was performed and size exclusion chromatography was conducted with the supernatant using an ÄKTA purifier system (GE Healthcare, Chicago, IL) and an XK50/100 column packed with Sepharose 6FF. The fractions containing the methacrylated porcine gastric mucin (PGM-MA) were detected by the UV absorption at 280 nm, collected, lyophilized, and stored at  $-80$  °C until further use.

### 2.3. Preparation of the Bio-Ink

To prepare the bio-ink, lyophilized PGM-MA was dissolved in ddH<sub>2</sub>O at a concentration of 8 % (w/v), vortexed for 1 min, and thoroughly mixed with a magnetic stirrer (at 300 rpm) at 4 °C for 12 h. In parallel, 8% (w/v) Laponite XLG (BYK-Chemie GmbH, Wesel, Germany) was dissolved in ddH<sub>2</sub>O as follows: First, ddH<sub>2</sub>O was cooled down on ice for 5 min and then agitated on a magnetic stirrer at 1500 rpm until a clear swirl was created. The Laponite powder was then slowly added, and the clay particles were allowed to swell for 16 h. Then, the PGM-MA solution and the Laponite solutions were mixed in a 1:1 ratio and homogenized at 1200 rpm (high speed homogenizer FSH-2A, Vevor Corporation GmbH, Köln, Germany) for 2 min. For control solutions that were supposed to contain only one of these two components,

the exact same procedure was conducted, but the respective stock solution was mixed in a 1:1 ratio with ddH<sub>2</sub>O.

#### 2.4. Curing of the Bio-Ink via Free Radical Polymerization

The photoinitiator 2-hydroxy-4'-(2-hydroxyethoxy)-2-methylpropiophenone (Irgacure 2959; Sigma-Aldrich) was used to enable UV-induced crosslinking of the PGM-MA molecules; previously, this chemical was already shown to be a suitable agent that guarantees both low cytotoxicity and efficient crosslinking.<sup>[33]</sup> Here, an aqueous solution of 80% (v/v) ethanol containing 100 mg mL<sup>-1</sup> Irgacure 2959 was added to the prepared bio-ink such that a final Irgacure concentration of 1 mg mL<sup>-1</sup> was obtained. Immediately afterward, the mixture was homogenized again by stirring at 1200 rpm for 2 min (to obtain a homogeneous dispersion of the photoinitiator) while avoiding any light exposure. Photo-crosslinking of the PGM-MA molecules (which is responsible for gelation of the PGM-MA solutions) was conducted by exposing the solutions to UV light (365 nm wavelength,  $\approx 10$  mW cm<sup>-2</sup>; M365L2, Thorlabs GmbH, Lübeck, Germany) as described in the individual experiments.

#### 2.5. Rheometry

To evaluate the material characteristics of the different formulations used in this study, several rheological measurements were conducted on a commercial shear rheometer (MCR102, Anton Paar, Graz, Austria) using a plate-plate geometry. To allow for illumination of the samples (where desired), a transparent bottom plate (P-PTD200/GL, Anton Paar) was chosen that is permeable for the transmission of UV light; furthermore, a UV lamp (M365L2, Thorlabs GmbH, Bergkirchen, Germany) was mounted below this transparent bottom plate. All measurements were conducted at a temperature of 25 °C with a light-proof liquid trap placed around the measuring chamber; this liquid trap not only protected the sample from drying but also prevented uncontrolled curing induced by environmental UV light. The gap size between the bottom plate and the measuring head (PP25, Anton Paar) was set to 300  $\mu$ m for all experiments, and a sample volume of 250  $\mu$ L was used.

To determine the viscosity of the different material formulations before curing, shear-rate ramps ranging from 10<sup>3</sup> to 10<sup>0</sup> s<sup>-1</sup> were measured. To follow the time-dependent curing process of the materials, the storage modulus,  $G'$ , and the loss modulus,  $G''$ , were determined at a constant frequency of 1 Hz while applying a constant torque of 5  $\mu$ Nm. First, a baseline was obtained for 5 min without UV exposure; then measurement points were recorded for 15 min of UV illumination. In the experimental setup using a glass plate to carry the samples, the intensity of UV light in the sample plane was  $\approx 7.3$  mW cm<sup>-2</sup>. To assess the viscoelastic behavior of the samples before and after the curing process more in detail, the storage ( $G'$ ) and loss ( $G''$ ) moduli were determined in response to a constant shear strain, and oscillation frequencies ranging from 0.1 to 10 Hz were applied. For samples that were not cured yet, the shear strain was set to the 1.5-fold value of the averaged shear strain obtained when applying an oscillatory torque of 0.5  $\mu$ N m (those values are obtained for every sample

type in pre-tests). For cured samples, the constant strain was set to the strain values observed during the five last data points of the curing measurements (see above).

#### 2.6. Filament Drop Test and Filament Shape Evaluation

To investigate the required pressure to be applied to extrude the bio-ink during the printing process, a filament drop test was conducted. Here, extrusion pressure was applied in a static printer configuration, i.e., without any movement of the nozzle. The distance between the nozzle and the printing bed was set to 40 mm. Lateral images of the formed filament (or fragments of a filament) were captured using an EOS M50 system camera (Canon, Tokyo, Japan) in high-speed mode.

The identified pressure was then applied to print 15 filaments each at different moving speeds of the nozzle. Therefore, the nozzle height was calibrated to the printing bed and five straight lines (2 cm each) were printed. Images were again captured using an EOS M50 system camera (Canon), and those images were analyzed using imageJ2 (version 2.3.0/1.53q). Then, the width of each filament was measured at five random positions.

#### 2.7. Height Increase Measurements

To determine the increase in sample height achieved when printing the mucin-based bio-ink, cylinders with a diameter of 5 mm were printed (Bio X, Cellink, Gothenburg, Sweden) with a 25G nozzle moving at a lateral speed of 20 mm s<sup>-1</sup>. An extrusion pressure of 80 kPa was applied, a layer height of 0.3 mm was targeted, and an infill density of 45 % with a rectangular pattern was selected. After extrusion of each layer, the sample was cured for 30 s with the in-built UV module for irradiation with 365 nm (BIO X Photocuring Toolhead 365 nm, Cellink). In addition, after printing each layer, a lateral photo was captured from the printed object, and the obtained images were analyzed using ImageJ2 (version 2.3.0/1.53q). To do so, two lines were manually fitted to approximate the bottom and top edge of the printed samples, respectively. The distance of those (mostly parallel) lines was then measured at the horizontal middle point of the sample.

#### 2.8. Swelling Experiments

To assess the swelling behavior of the cured bio-ink, samples were prepared as described above (including the addition of the photo-initiator), and the wells of a 96-well plate were filled with 100  $\mu$ L of the respective bio-ink solution. The samples were then cured by UV-illumination as described above. Directly after curing, the samples were weighed using a micro-balance (XSE205 Dual Range, Mettler Toledo, Columbus, USA). Then, they were placed into a tube filled with 5 mL of either ddH<sub>2</sub>O or ddH<sub>2</sub>O with different salt concentrations such that the samples were fully covered with liquid at all times. After an incubation time of 5 days (a time span that should be sufficient for the samples to reach an equilibrium state<sup>[34]</sup>), the hydrogel samples were gently blotted from each side to remove excess water, air-dried for 5 min and again weighed.



## 2.9. Unconfined Compression Tests

Unconfined compression tests of cured samples were performed on a commercial rheometer (MCR102, Anton Paar) equipped with a standard bottom plate (P-PTD200/AIR, Anton Paar) and a planar PP08 measuring head (PP08-5681, Anton Paar). The samples were prepared in the wells of a 48-well plate to perfectly match the dimension of the measuring head. Therefore, 200  $\mu\text{L}$  of a bio-ink were filled into a well and cured with UV light (365 nm wavelength,  $\approx 10 \text{ mW cm}^{-2}$ ; M365L2, Thorlabs GmbH) for 15 min; this time span was found (based on macrorheological measurements) to be more than sufficient to reach the final gel strength. The cured samples were gently removed from the wells and placed onto the bottom plate of the rheometer. After resetting the normal force before each measurement, the measuring head was lowered until a gap of 4 mm was reached (measured between the measuring head and the bottom plate). Then, the measuring head was further lowered with a constant speed of  $v = 10 \mu\text{m s}^{-1}$  and the normal force  $F_N$  was recorded over time. For each sample, the gap size at which the first full contact between the measuring head and the sample occurred was noted—and this distance represents the individual sample height that is later on needed to calculate the axial strain.

From the obtained curves, the compression modulus was calculated as follows: First, the obtained normal force was converted into a normal pressure according to  $p = F_N \times (\pi \times r^2)^{-1}$ , with  $r = 7.965 \text{ mm}$ . Then, the continuously shrinking gap size  $\Delta d_g$  was converted into axial strain values according to  $\gamma = \Delta d_g \times h_s^{-1}$ ; here,  $h_s$  denotes the individual sample thickness that was determined as described above. Afterward, to only consider the linear regime of the obtained curve, the 20 points measured directly before sample breakage were discarded, and a linear, least squares regression curve was fitted to the remaining data using the software GraphPad Prism (Prism 9 for macOS; Version 9.3.1 (350), December 7, 2021; GraphPad Software LLC; San Diego, CA). Finally, the slopes of those regression lines represented the compression moduli of the respective samples.

## 2.10. Cytotoxicity Tests

For those tests, an established human epithelial cell line (HeLa) was used as a model system. Those HeLa cells were cultivated in Minimum Essential Medium Eagle (MEM; Sigma-Aldrich) supplemented with 10% (v/v) fetal bovine serum (FBS; Sigma-Aldrich),  $2 \times 10^{-3} \text{ M}$  L-glutamine solution (Sigma-Aldrich), 1% (v/v) non-essential amino acid solution (NEAA; Sigma-Aldrich), and 1% penicillin/streptomycin (Sigma-Aldrich). The cells were then cultured at  $37^\circ\text{C}$  and 5%  $\text{CO}_2$  in a humidified atmosphere.

To analyze cell/bio-ink interactions and to investigate possible cytotoxic effects of the different bio-ink formulations, samples were prepared as described for the swelling experiments; then, cell-based assays according to ISO 10993 were conducted. In brief, the cured bio-ink specimens were immersed in the corresponding cell culture medium for 24 h at  $37^\circ\text{C}$  to allow for loosely integrated gel components to leach out. Afterward, a WST-1 assay was used to assess the cytotoxicity of this “leaching” medium. For this step, HeLa cells were seeded into the wells of a 96-well plate (5000 cells/well) and incubated for 24 h at  $37^\circ\text{C}$ . Subsequently,

the cell culture medium was removed from the 96-well plate and replaced with sterile filtrated “leaching” medium (as a control group, cells were incubated with fresh cell culture medium). After 24 and 48 h of incubation, respectively, the leaching medium was replaced with a 2% (v/v) WST-1 solution (Sigma-Aldrich). After an incubation time of 45 min, the absorbance values of the samples were obtained at a wavelength of 450 nm and at a reference wavelength of 630 nm using a microplate reader (ABSPPlus, Molecular Devices, Wokingham, Berkshire, UK). The cellular viability was then calculated by normalizing the absorbance value obtained for test groups to that of the control group.

## 2.11. Cell Adhesion Tests

The attachment propensity of cells onto the bio-inks was analyzed by confocal laser scanning microscopy (CLSM; SP8, Leica; equipped with a  $10\times$  lens). For cell staining, the dye CellTracker Red CMTPX (excitation/emission wavelength: 577/602 nm; Thermo Fisher Scientific) was chosen; cells were stained prior to seeding them onto the bio-inks. To do so, HeLa cells were cultivated as described above, harvested, and resuspended in a serum-free medium (containing  $10 \times 10^{-6} \text{ M}$  of the dye) for 30 min. Then, the cells were washed twice by Dulbecco’s phosphate-buffered saline (DPBS, pH 7.4; Sigma-Aldrich) and resuspended in the corresponding standard cell culture medium. Subsequently, the cells were seeded (10000 cells per well) into eight-well chambers (80826, Ibidi, Gräfelfing, Germany) containing one of the bio-inks and incubated for 24 h at  $37^\circ\text{C}$ . For each bio-ink variant, three sample replicates were prepared; empty wells were used as a control group. Then, using CLSM, 3D image stacks of the samples were collected by moving the focal plane (pinhole size = 1 airy disk) from the bottom of the samples to their top (nominal z-step size:  $20 \mu\text{m}$ ). The software Leica Application Suite X (Leica) was used for processing the 3D image stacks, and cells were counted using ImageJ2 (version 2.3.0/1.53q).

## 2.12. Bacterial Adhesion Tests

The adhesion of bacteria to bio-ink samples was evaluated for the strains *S. epidermidis* ATCC 14990 and *E. coli* ATCC 25922. Bio-ink samples were prepared in well plates as described above, sterilized by exposing them to UV light at a wavelength of 254 nm for 2 h, and subsequently washed thrice with 70% (v/v) ethanol. The bacterial strains were kept frozen in cryovials and were reconstituted in sterile phosphate buffered saline (PBS, pH 7.4). Afterward, these bacterial suspensions were inoculated at a concentration of  $10^8 \text{ CFU mL}^{-1}$  on the sterilized bio-ink samples and incubated at  $37^\circ\text{C}$  for 3 h. After incubation, the samples were thoroughly washed thrice with sterile PBS to remove the non-adherent bacteria. To detach the adherent bacteria from the bio-ink samples, the samples were transferred from the well plate into tubes and vortexed in sterile PBS for 1 min. For each sample, the bacterial suspension generated with this method was serially diluted and plated onto Chapman Agar (Sigma-Aldrich) in duplicates using the Interscience easySpiral Dilute (Interscience, France). Then, to determine the number of adherent bacteria,

those agar plates were incubated at 37 °C for 72 h, and the number of grown colony forming units (CFU) was counted using the Scan 500 Colony Counter (Interscience, France).

### 2.13. Lipid Depletion Assay

For the lipid depletion tests, 250 µL of the different samples (pure Laponite, pure PGM-MA, and the final bio-ink formulation containing both components) were injected into the wells of a 48-well plate and they were cured in situ. Then, 250 µL DPBS containing  $25 \times 10^{-6}$  M fluorescently labeled 1,2-di-(9Z-octadecenyl)-sn-glycero-3-phosphoethanolamin (DOPE-Rhodamine; Avanti Polar Lipids, Alabama, USA) lipids were added to each well. After an incubation step at RT for 3 h while gently shaking the samples, 100 µL of the liquid solution were removed from each well and the fluorescence intensity of the solutions was measured using a plate reader (ex.: 575 nm, em.: 595 nm; Varioskan Lux, Thermo Fisher Scientific, Waltham, MA).

### 2.14. Cytokine Release from Macrophages

The immune response to the different bio-ink formulations was evaluated by determining the cytokine expression of monocyte-derived macrophages. The human cell line U937 (ATCC, American Type Culture Collection, Manassas, VA) was kept in culture medium composed of RPMI 1640 medium (Gibco, Life Technologies, Paisely, UK) supplemented with 10% (v/v) fetal calf serum (Gibco),  $2 \times 10^{-3}$  M L-glutamine (Gibco),  $1 \times 10^{-3}$  M sodium pyruvate (Gibco), 1 U mL<sup>-1</sup> penicillin and 1 µg mL<sup>-1</sup> streptomycin (Gibco). The cells were then differentiated into M0 macrophages by culturing them in cell culture medium supplemented with  $100 \times 10^{-9}$  M phorbol 12-myristate 13-acetate for 72 h, and they were subsequently allowed to rest in fresh culture medium for 24 h. They were then seeded at a density of 900 000 cells cm<sup>-2</sup> onto the samples, and after 72 h of incubation at 37 °C with 5 % CO<sub>2</sub>, the cytokine concentration in the supernatant was evaluated. Quantification of the released proinflammatory (TNF-α and IL-6) and anti-inflammatory (IL-10 and TGF-β) cytokines was performed with the DuoSetELISA kit (R&D Systems, Minneapolis, MN) following the manufacturer's instructions using a multimode microplate reader (Spark, Tecan, Männedorf, Switzerland).

### 2.15. Statistical Analysis

Tests for statistical significance were performed for the cytokine expression data. A normal data distribution was tested for each sample with a Lilliefors test, and a two-sample *F*-test was used to check for equal variances. To test for significant differences between normally distributed samples, a two-sample *t*-test was applied when homogeneity of variances was met, whereas a Welch's *t*-test was performed for unequal variances. For samples that were not normally distributed, a Wilcoxon–Mann–Whitney test was performed. All statistical analyses were performed using Matlab (version R2019a, MathWorks, Natick, MA), and differences were considered statistically significant if a *p*-value below 0.05 was obtained.

### 2.16. Statement of Ethics Approval

Approval of ethics is not required for the experiments conducted in this paper.

## 3. Results and Discussion

### 3.1. Bio-Ink Development and Rheological Evaluation

For all bio-ink formulations discussed here, porcine gastric mucin (PGM) functionalized with methacrylic anhydride (= PGM-MA, Figure 1) constitutes the base component. Fourier transform infrared spectroscopy confirms the successful methacrylation of the mucin: when comparing the spectra obtained for pure PGM to those obtained for PGM-MA, we find that the conjugated mucins show an additional peak at a wavenumber of  $\approx 1718$  cm<sup>-1</sup>, which corresponds to the carbonyl residues of the methacryloyl groups (see Figure S1, Supporting Information).<sup>[35]</sup> An aqueous solution containing 4 % (w/v) PGM-MA shows shear-thinning properties with viscosities slightly above 100 mPa s and exhibits frequency-dependent characteristics typical for a viscoelastic fluid (Figure 2a,b).

Those rheological properties critically determine the suitability of a material for 3D printing. The viscosity, for instance, quantifies the resistance of a fluid to flow. This resistance, which results from internal friction, hinders movements in response to applied stress—and such a scenario occurs when extruding the material through a printing head. Whereas for simple, Newtonian fluids, the viscosity is independent of the shear rate, for polymer solutions, this is usually not the case: for low shear rates, entanglements between the polymers lead to a high viscosity; however, with increasing shear rates, the polymers align with the flow and the viscosity decreases. This behavior, referred to as shear-thinning, can be beneficial for 3D printing: As long as the material remains in a cartridge without any forces applied, its tendency to spontaneously flow through the nozzle is low. In contrast, once pressure is applied, the ink can be easily extruded.

In addition to the viscosity, a biopolymer-based material can typically be characterized regarding its viscoelasticity, i.e., its frequency-dependent ability to exhibit both, viscous and elastic behavior when subjected to stress. To allow for proper extrudability, an ink material should behave like a viscoelastic fluid; however, once printed, the material response should switch to an elasticity-dominated state to allow for maintaining the created shape. To achieve this transition, a curing strategy is usually required. For the initially viscosity-dominated mucin-based bio-ink, the methacryloyl groups on the PGM-MA allow for photo-initiated covalent crosslinking of the mucin glycoproteins via free-radical polymerization<sup>[36]</sup>: When supplemented with a suitable photo-crosslinker, polymerization of the PGM-MA molecules can be initiated by UV irradiation (Figure 2c), and this leads to a rapid and strong alteration of the material properties. The initially liquid solution switches into a gel state within 20 s; now, the material response is dominated by elastic properties. Within  $\approx 4$  min of curing, the elastic modulus of this gel reaches a plateau value of  $\approx 0.8$  kPa. After completed curing, this value is stable and quite constant over the whole frequency spectrum probed here (see Figure S2, Supporting Information), which is typical for a covalently cross-linked (bio)polymer gel.<sup>[37]</sup>

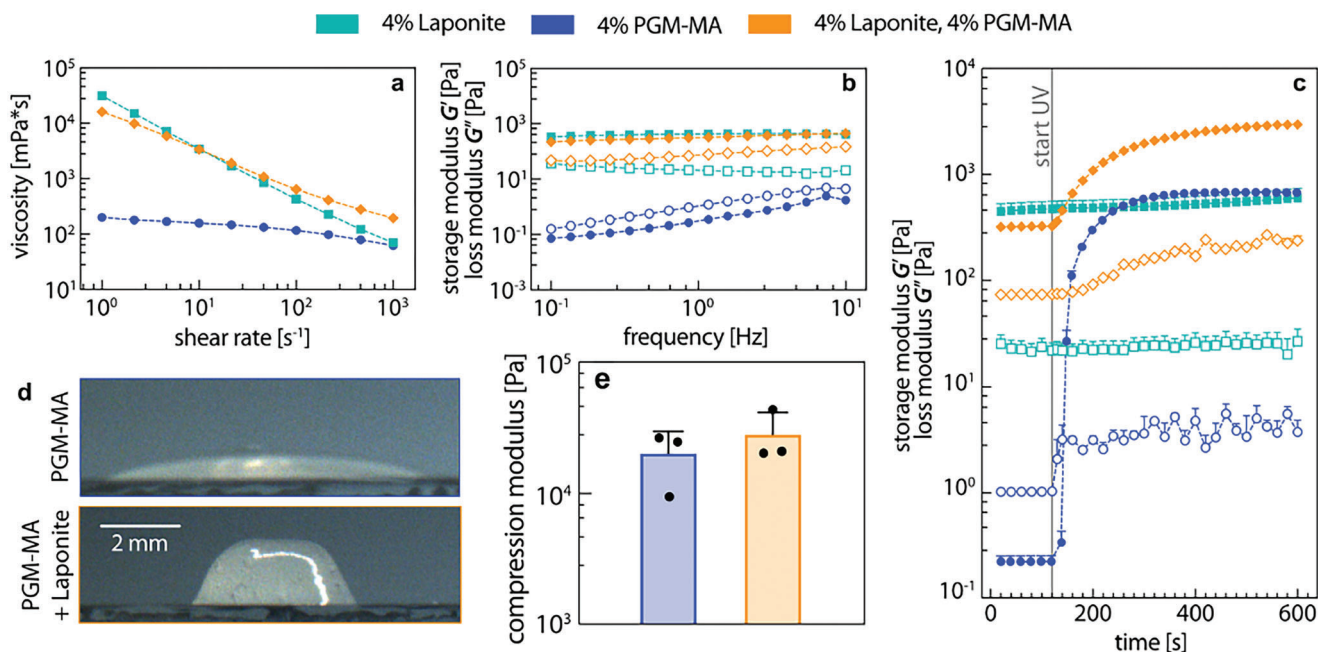


**Figure 2.** Mechanical characterization of different bio-ink formulations. a) Viscosities of the materials at different shear rates and the viscoelastic moduli measured b) over a frequency spectrum or c) at a fixed frequency during UV irradiation. d) Images of four layers of bio-ink printed without any curing and e) the compression moduli of cured ink samples. Error bars denote the standard error of the mean as obtained from  $n \geq 3$  measurements. If not visible, the error bars are smaller than the symbol size.

Using those UV-curable mucin solutions as a basis component, we next tune the rheological properties of the bio-ink to optimize it for extrusion-based additive manufacturing. For such a 3D-printing application, as stated above, the viscosity of the mixture is an important parameter for two reasons: first, it influences the extrusion flow and defines the required extrusion pressure; second, the viscosity determines how fast a liquid material spreads on the printing bed, i.e., how long the material can (at least to a certain degree) maintain its shape before covalent cross-links are introduced by UV-illumination. Whereas the second aspect benefits from a high viscosity of the ink, a strongly viscous ink limits the achievable moving speeds during the printing process and reduces the smoothness of the printed filaments. Thus, to ensure good printability, the ink material should exhibit shear-thinning characteristics. Without additives, a bio-ink comprising only PGM-MA shows this desired shear-thinning behavior; yet, overall, its viscosity is rather low, which calls for adjustment. Moreover, after printing, the PGM-MA solution is not able to maintain its shape (Figure 2d), which further underscores the need to improve the viscous properties of the bio-ink.

Such control over the viscosity of a complex fluid can be achieved by different strategies; examples include using a thermo-responsive additive or another mechanical adjuvants that acts as a stabilizing support material. To avoid subjecting the biopolymeric PGM-MA to unnecessary thermal stress, we choose to adjust the viscosity of the fluid by adding a stabilizing agent, i.e., either methylcellulose or nanoclay (Laponite XLG). Indeed, either of those two additives successfully increases the viscosity of the bio-ink by several decades while maintaining the desired shear-thinning properties (Figure 2a and Figure S3, Supporting Information). However, the nanoclay additive outperforms

methylcellulose in several aspects: First, the nanoclay can be thoroughly mixed with the mucin, and this allows for higher additive concentrations to be used while still achieving a homogeneous ink formulation. Second, different from what is achieved with methylcellulose, the nanoclay-containing bio-ink forms a viscoelastic gel even before curing (Figure 2a and Figure S3, Supporting Information). This particular property turns out to be important when comparing the extrusion performance of the two bio-ink variants: a certain elasticity of the material is extremely helpful to achieve a sufficiently high intrinsic stability of the printed product until the covalent cross-links generated by UV-treatment are established (Figure 2d). Hence, for further experiments, only the nanoclay-based ink variant is considered. With this particular bio-ink formulation, the curing time of the material is very similar to that of pure PGM-MA solutions, and the elastic properties of the final, cured material are slightly increased to  $\approx 2$  kPa. As a material to be used in a biomedical context, the mechanical properties of the bio-ink strongly influence the ability of the material to integrate well into soft tissue. Here, in addition to shear stress, another relevant type of mechanical load is compression. When conducting unconfined compression tests with the bio-ink, compression moduli of around 10–11 kPa are observed (Figure 2e; for stress–strain curves, please refer to Figure S4, Supporting Information). Thus, the elastic moduli obtained from the two mechanical tests are in a similar range as values previously reported for mammalian soft tissue and organs.<sup>[38]</sup> A difference to such soft tissue is observed when subjecting the cured bio-ink to large-amplitude strain. The cured ink shows strain weakening properties (for details, please refer to Section S5, Supporting Information), whereas soft tissues usually exhibit strain hardening properties. For some purposes, however, strain

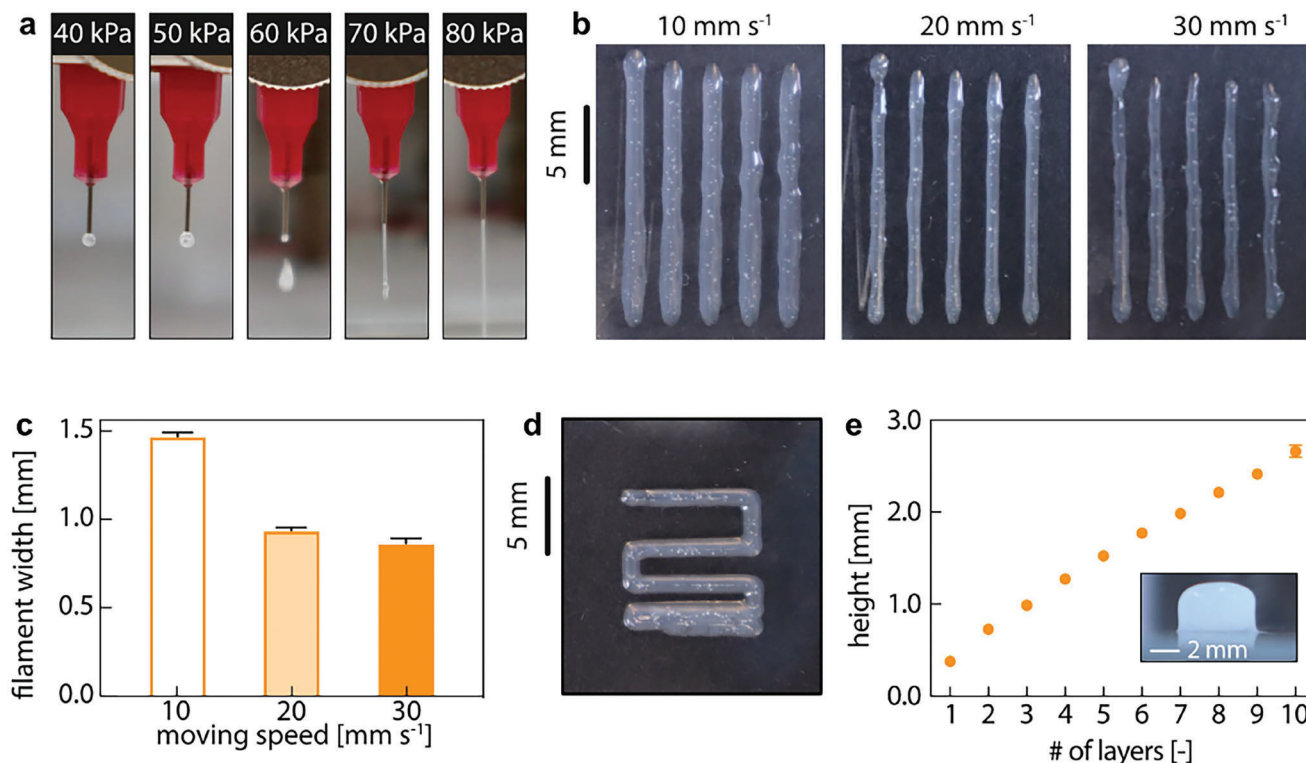


**Figure 3.** 3D printing of the mucin-based composite bio-ink. a) A drop-test was conducted to identify a suitable pressure level for extrusion of the bio-ink. b,c) Filaments were printed at different moving speeds and their thickness was quantified. d) A meander pattern was printed with 80 kPa and a moving speed of 20 mm s<sup>-1</sup> to visualize the printing accuracy. e) Finally, the height increase per printed layer was monitored. Error bars denote the standard error of the mean as obtained from  $n = 15$  (b) and  $n = 3$  (d) samples.

weakening material properties can be beneficial, as they, for instance, can facilitate cell migration.<sup>[39]</sup>

Next, the performance of this improved bio-ink formulation (containing 4% Laponite and 4% PGM-MA) is evaluated in more detail using a fused deposition modeling system. Therefore, we first aim at identifying a suitable pressure to be applied during the printing process. Here, the goal is to extrude the bio-ink into a continuous filament without any interruption. When performing a filament drop test (Figure 3a), we find that pressure levels of 40 and 50 kPa, respectively, are not sufficient to extrude the bio-ink; here, only a small droplet is formed at the needle tip without achieving further extrusion. At higher pressure levels of 60 and 70 kPa, respectively, we observe the extrusion of multiple individual droplets and small filament-like sections, respectively; indeed, pressure levels of 80 kPa are required to obtain continuous filaments. Hence, for all further procedures, an extrusion pressure level of 80 kPa is selected.

When we use this pressure level to extrude filaments at three different moving speeds, we find that the slowest moving speed (10 mm s<sup>-1</sup>) leads to thick, poorly defined filaments; however, the filament shape and its reproducibility greatly improve when doubling this moving speed to 20 mm s<sup>-1</sup> (Figure 3b,c). When the moving speed is further increased to 30 mm s<sup>-1</sup>, the thickness of the filaments is only slightly reduced, but the shape of the filaments becomes more irregular and asymmetric. Hence, we identify a moving speed of 20 mm s<sup>-1</sup> to be best suited for the used setup used here. As depicted in Figure 3d, with the identi-

fied printing parameters, structures can be printed with a resolution of approximately 1 mm.

Having identified suitable printing parameters for the developed bio-ink, we print a cylinder with a diameter of 5 mm and monitor the increase in sample height after extruding and curing each layer. As desired, when increasing the number of printed layers, we observe a linear increase of the sample height (Figure 3e), and a nicely shaped cylinder is generated (Figure 3e, inset). Thus, this first printing trial already indicates that the developed ink material is indeed able to generate a 3D-printed sample of desired shape with sufficient intrinsic stability.

### 3.2. Bio-Ink Swelling Is Sensitive toward the Ionic Content of the Liquid Environment

Having tested the performance of the bio-ink in a 3D printing setup, we next investigate swelling behavior of different cured ink samples. To do so, cylindrical samples are created by cast-molding and immersed into liquid environments supplemented with different amounts of salt, and their change in weight after 5 d of storage is determined (Figure 4a; for exemplary pictures, please refer to Section S6, Supporting Information). Those swelling tests are only conducted with PGM-MA-containing samples, since pure Laponite specimens are not able to properly maintain their shape when immersed into a water-based fluid. For bio-ink samples stored in ddH<sub>2</sub>O, a strong swelling behavior



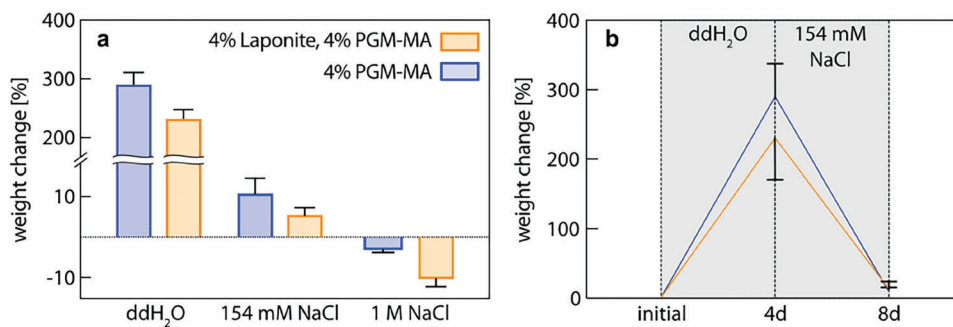


**Figure 4.** Swelling behavior and compressive strength of different bio-ink formulations. a) Weight change that cured bio-ink specimens undergo when exposed to liquid environments with different salt concentrations and b) its reversibility. Error bars denote the standard error of the mean as obtained from  $n \geq 3$  samples.

is observed: We find an increase in weight of nearly 300 % for pure PGM-MA specimens and of 250% for samples containing both, PGM-MA and Laponite. This strong swelling is probably driven by the repulsive electrostatic forces acting between the strongly anionic mucin molecules (via electrophoretic light scattering, we determine the zeta potential of the PGM-MA macromolecules to be  $-26.1 \pm 0.4$  mV; for details regarding the method, see Section S7, Supporting Information). With increasing salt concentrations, sample swelling is drastically reduced or even converted into shrinkage: We determine sample weight increases of only 10% for cured samples immersed into a physiological saline solution, whereas cured samples incubated in a 1 M NaCl solution shrink by up to 10%. These findings agree with our notion that electrostatic repulsion forces drive sample swelling: With increasing NaCl content, the solubilized salt ions will increasingly shield the negatively charged groups on the mucin molecules (Debye-screening), which allows for a much more compact state of the bio-ink sample.

Consistent with this picture, we find that sample swelling is reversible: when a freshly cured sample (which was prepared in ddH<sub>2</sub>O as described in the Experimental Section) is first immersed into ddH<sub>2</sub>O for 4 d (until full swelling is achieved) and then placed into water containing physiological NaCl concentrations ( $154 \times 10^{-3}$  M) for another 4 d, the sample nearly fully recovers its initial volume. In other words, it is possible to adjust the volume of printed structures created with this mucin-based bio-ink by incubating them in aqueous solutions containing different ion concentrations. Importantly, even in their swollen state, the printed samples are stable and do not break up into fragments.

### 3.3. The Mucin-Based Bio-Ink Combines Good Biocompatibility with Anti-Biofouling Behavior

To be used in a biomedical context, it is essential that the cured objects generated from the bio-ink exhibit sufficient biocompatibility. Hence, to test for putative cytotoxic effects, we perform a leaching test in combination with a WST-1 assay according to ISO 10993; for those experiments, epithelial HeLa cells are used as a model cell line. Within the time intervals tested here, i.e., for incubation periods of 24 and 48 h, respectively, no cytotoxic effects are detected: for all three bio-ink formulations, cell viability values above 80% are reached (Figure 5a). This posi-

tive finding is in line with previous studies that reported a non-toxic character for both, crosslinked mucin hydrogels<sup>[28a,34]</sup> and Laponite gels.<sup>[40]</sup> In addition to the biocompatibility of the cured bio-inks, we assess the ability of cells to adhere to the surface of cured ink samples by incubating cells on different samples (Figure 5b; for micro-topographical images of the sample surfaces and exemplary images of the cell adhesion tests, please refer to Sections S8 and S9, Supporting Information, respectively). As expected,<sup>[29c,40b,41]</sup> pure Laponite gels can be colonized by HeLa cells; in contrast, on pure PGM-MA gels, we find hardly any attached cells. Consistently, the addition of mucins to the Laponite gel considerably reduces the number of cells adhering to the gel. In other words, for the particular mixture ratio studied here, the cell experiments demonstrate that cured samples generated from the mucin-based bio-ink exhibit a cell-repellent behavior while maintaining a high biocompatibility.

Having shown that mucin strongly reduces the adhesion of cells onto the surfaces of cured bio-ink samples, we next aim at assessing the bacterial adhesion on those specimens. Several previous studies have demonstrated that surface coatings generated from mucin macromolecules can reduce bacterial adhesion,<sup>[29a,b]</sup> and it seems possible that mucin-enriched gels might be able to show a similar effect. To test this, we investigate the susceptibility of objects generated with the different bio-ink formulations to become colonized by bacteria. In detail, we incubate such specimens with bacterial suspensions of either *Staphylococcus epidermidis* or *Escherichia coli* and then determine the bacterial concentration adhering to the samples. For specimens comprising Laponite only, we find that approximately one out of 1000 bacteria from the inoculation solution adheres to the samples. This number, however, is further reduced by a factor of 10 for PGM-MA-containing samples (Figure 5c,d). Thus, these results demonstrate that objects printed with the mucin-based bio-ink exhibit good bacteria-repellent properties.

Last, to further test the anti-biofouling properties of the bio-ink, we perform a lipid depletion test. This test reveals that, whereas the lipids strongly adsorb to (or are absorbed into) pure Laponite gels, virtually no lipid binding was observed for the two mucin-containing gels (Figure 5e). In other words, the presence of mucin prevented the lipids from binding to the hydrogel matrix. These results underscore the good anti-biofouling performance of the bio-ink and indicate that, in addition to repelling bacteria, objects generated from the bio-ink exhibit

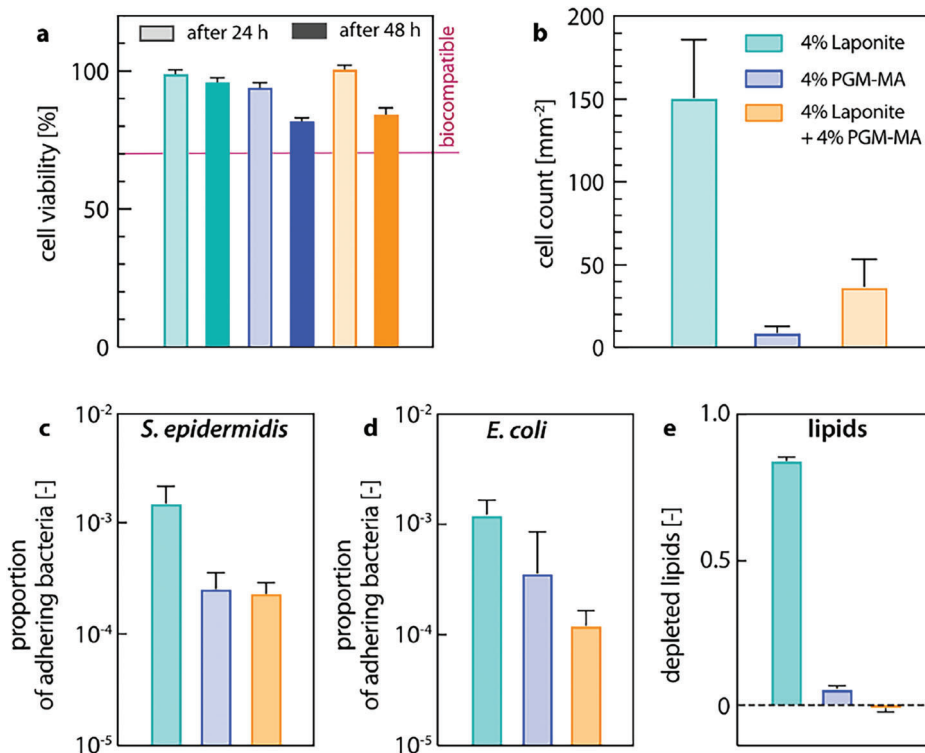


**Figure 5.** Biocompatibility and adhesion of cells, bacteria, and lipids to cured bio-ink samples. a) Biocompatibility of the cured bio-ink formulations as tested with a leaching test according to ISO10993. b) Adhesion of HeLa cells to the surfaces of cured bio-ink samples. c,d) The proportion of colony forming units (CFUs) attached to the bio-ink samples after incubation of the specimens with bacterial suspensions containing  $1.32 \times 10^8$  CFU mL<sup>-1</sup> of *S. epidermidis* or  $7.95 \times 10^8$  CFU mL<sup>-1</sup> of *E. coli*, respectively. e) Finally, the amount of lipids depleted from a solution by each material is depicted. Higher values denote high depletion of the lipids from the solution, hence high adsorption of the lipids onto or absorption into the bio-ink samples. Error bars denote the standard deviation as obtained from  $n = 4$  (a–d) samples and the standard error of the mean obtained from  $n = 3$  (e) samples, respectively.

strong anti-biofouling properties toward lipid-based structures, such as cellular debris.

### 3.4. Immune Responses Are Dampened by the Presence of Mucin in the Bio-ink

An artificial object that gets in contact with tissue surfaces elicits a foreign body response through its interaction with immune cells. This could entail several negative consequences resulting in rejection of the printed constructs. To evaluate the immune response triggered by each of the bio-ink components and the final bio-ink formulation, we assess the concentration of different pro- and anti-inflammatory cytokines secreted by macrophages that are seeded onto the different cured materials (Figure 6).

The cytokine secretion of macrophages that came into contact with pure Laponite hydrogels is significantly higher than that observed for macrophages seeded onto PGM-MA hydrogels. This result is consistent with prior findings concerning the immediate and long-term reactions of macrophages that were placed on mucin-derived materials: In those studies, it was demonstrated that mucin-based gels have a broad dampening impact on the cytokine expression of macrophages.<sup>[42]</sup> For the composite bio-ink formulation, we find differences between the pro- and anti-inflammatory cytokines: For the pro-inflammatory cytokines

(i.e., TNF- $\alpha$  and IL-6), the expression levels for the composite is in-between the secretion levels for the individual materials. In contrast, for the anti-inflammatory cytokines (i.e., IL-10 and TGF- $\beta$ ), the macrophages seeded onto the composite produce the lowest cytokine secretion. However, this could be explained considering the influence of the individual bio-ink components: As stated before, mucin molecules broadly dampen the secretion of both, pro- and anti-inflammatory cytokines. For Laponite, such a dampening effect was previously only observed for anti-inflammatory cytokines,<sup>[43]</sup> whereas no effect (neither an increasing nor a dampening one) was observed for pro-inflammatory cytokines.<sup>[44]</sup> Hence, the intermediate values obtained for TNF- $\alpha$  and IL-6 likely result from the combination of two materials that influence the cytokine expression differently. In contrast, for IL-10 and TGF- $\beta$ , both individual components dampen this immune response, which is why the combination of the two appears to result in a synergistic effect. Together, these results demonstrate that printed constructs created from mucin-derived bio-ink formulation have an immunomodulatory effect.

### 3.5. Challenges and Limitations

On the path to a clinical application of the developed bio-ink, several factors such as the sourcing of raw materials, reproducibility

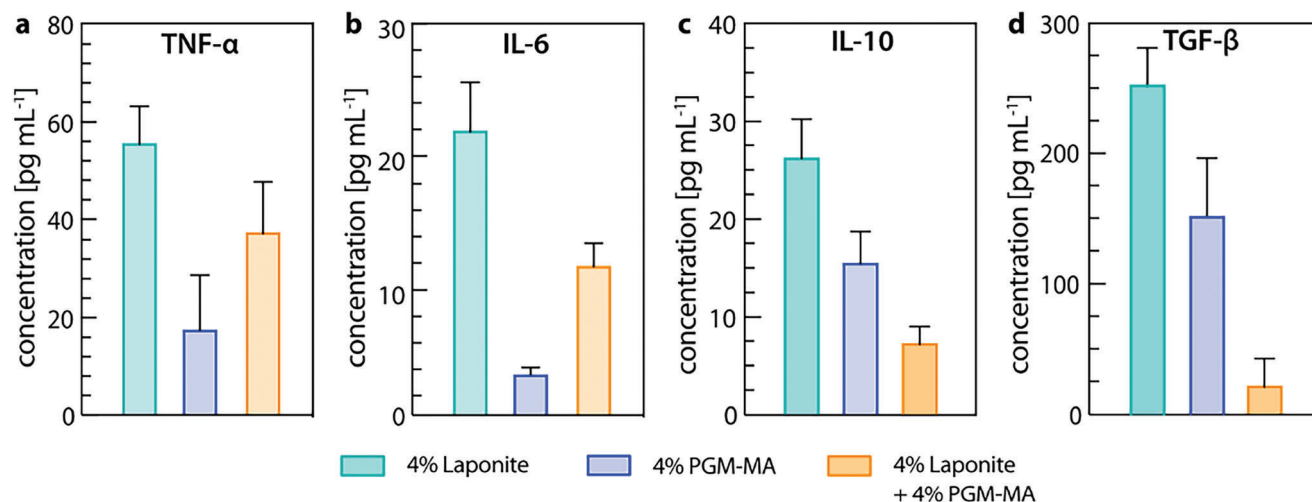


**Figure 6.** Cytokine expression on the different bio-ink formulations. Macrophages were seeded onto cured bio-ink samples of the individual components (i.e., Laponite hydrogels and PGM-MA hydrogels) and on the final bio-ink formulation. The secretion of the pro-inflammatory cytokines a) TNF- $\alpha$  and b) IL-6 and the anti-inflammatory cytokines c) IL-10 and d) TGF- $\beta$  are displayed. For all four cytokines, all three samples are significantly different from each other based on a  $p$ -level of 0.05 (for simplicity, no asterisks were added to these figures).

of the formulation, and conformity with relevant regulations have to be considered. Whereas we here successfully prepared and tested the bio-ink on a laboratory scale, producing the material on a larger scale may come with challenges. In this study, commercial PGM Type II (Sigma-Aldrich) was chosen due to its good availability; and even with this only crudely purified mucin product, we were able to achieve a very good functionality of the bio-ink. However, using mucin variants with higher purity, such as partially purified PGM Type III (Sigma-Aldrich) or in-lab purified PGM, might help to reduce batch-to-batch variations (for a detailed comparison of commercial and in-lab purified mucin variants, please refer to Marczynski et al.<sup>[32]</sup>). Of course, additional purification steps render the preparation procedure more costly and time consuming and typically reduce the yield. However, for in-lab purified mucins, recent process modifications were able to considerably increase this yield of high-quality mucins while significantly reducing the process times and costs.<sup>[45]</sup>

In addition to ensuring consistent and high quality, for a product to be used in a medical context, it has to conform with regulations regarding sterility. However, for a material containing components of animal origin, sterility cannot be guaranteed—even after careful purification. Hence, sterilization treatments using heat, radiation, or chemicals have to be applied, and this could compromise the physicochemical or structural properties of the biomolecule component of a bio-ink. However, for the bio-ink formulation introduced here, this point is not problematic: previous studies demonstrated that mucins are able to tolerate several harsh decontamination treatments without suffering significant functional impairment or structural degradation.<sup>[46]</sup>

Last, the presented bio-ink formulation and the used printing process could be further refined to enhance the printing accuracy and to allow for creating more complex and more detailed structures. Currently, the achieved resolutions are in the range of 1 mm, and this resolution might be improved by integrating additional stabilizing agents. Moreover, when refining the bio-ink formulation in future studies, the impact the inner diameter of

the printing head has on the printing outcome should be considered. Smaller needles could be used to improve the resolution of the printed objects, whereas bigger needle gauges might be beneficial for depositing thicker filaments to achieve better structural integrity.

## 4. Conclusion

The bio-ink formulation developed in this study combines functionalized mucins with Laponite, and cured objects generated from this ink exhibit mechanical properties partially similar to those of soft tissue, excellent biocompatibility, strong anti-biofouling properties, and tunable cell adhesion behavior. This unique combination of characteristics renders this bio-ink a promising candidate for a wide range of applications such as tissue engineering and regenerative medicine (e.g., for creating soft tissue replacements). Future refinements of the bio-ink formulation could further enhance its printing performance so it can be used to create more complex and more detailed structures. Moreover, such a mucin-based bio-ink could also find applications in drug delivery and wound healing: mucin-based gels have previously been demonstrated to be suitable carriers for drug release,<sup>[28a,47]</sup> and Laponite was shown to promote wound healing by releasing magnesium ions.<sup>[40a,48]</sup> In addition, owing to the ink's tunable cell adhesion and anti-biofouling properties, it could also be used to create tailored, biocompatible interfaces between living tissue and artificial objects, e.g., prosthetics or implantable medical devices. This broad range of possible applications indicates the high versatility of this bio-ink and its usefulness as a biomaterial for biomedical engineering.

## Supporting Information

Supporting Information is available from the Wiley Online Library or from the author.

## Acknowledgements

This project was funded by the Federal Ministry of Education and Research (BMBF) and the Free State of Bavaria under the Excellence Strategy of the Federal Government and the Länder through the ONE MUNICH Project Munich Multiscale Biofabrication. The authors thank Matthias Marczyński and Marvin Ertelt for their advice with chemical issues and Preethika Chivukula for conducting pilot experiments.

Open access funding enabled and organized by Projekt DEAL.

## Conflict of Interest

The authors declare no conflict of interest.

## Author Contributions

C.A.R., S.M., and O.L. designed the experiments; C.A.R., D.F., and S.M. performed the experiments. C.A.R. analyzed data. The manuscript was written by O.L. and C.A.R., which was critically revised by all authors.

## Data Availability Statement

The data that support the findings of this study are available from the corresponding author upon reasonable request.

## Keywords

cell adhesion, immune-modulation, nanoclay, photo-crosslinking, rheology

Received: May 8, 2023

Revised: July 10, 2023

Published online: July 25, 2023

- [1] a) V. Egorov, U. Gulzar, Y. Zhang, S. Breen, C. O'dwyer, *Adv. Mater.* **2020**, *32*, 2000556; b) M. A. S. R. Saadi, A. Maguire, N. T. Pottackal, M. D. S. H. Thakur, M. M. D. Ikram, A. J. Hart, P. M. Ajayan, M. M. Rahman, *Adv. Mater.* **2022**, *34*, 2108855; c) L. U.-Y. U. Zhou, J. Fu, Y. He, *Adv. Funct. Mater.* **2020**, *30*, 2000187.
- [2] a) P. D. C. Costa, D. C. S. Costa, T. R. Correia, V. M. Gaspar, J. F. Mano, *Adv. Mater. Technol.* **2021**, *6*, 2100168; b) R. L. Truby, J. A. Lewis, *Nature* **2016**, *540*, 371; c) Q. Ge, Z. Chen, J. Cheng, B. Zhang, Y.-F. Zhang, H. Li, X. He, C. Yuan, J. Liu, S. Magdassi, S. Qu, *Sci. Adv.* **2021**, *7*, eaba4261; d) T. Erps, M. Foshey, M. K. Lukovic, W. Shou, H. H. Goetzke, H. Dietsch, K. Stoll, B. Von Vacano, W. Matusik, *Sci. Adv.* **2021**, *7*, eabf7435.
- [3] a) L. E. Murr, *J. Mater. Res. Technol.* **2020**, *9*, 1087; b) N. Noor, A. Shapira, R. Edri, I. Gal, L. Wertheim, T. Dvir, *Adv. Sci.* **2019**, *6*, 1900344; c) S. N. Economidou, M. J. Uddin, M. J. Marques, D. Douroumis, W. T. Sow, H. Li, A. Reid, J. F. Windmill, A. Podoleanu, *Addit. Manuf.* **2021**, *38*, 101815.
- [4] a) S. Chen, W. S. Tan, M. A. Bin Juhari, Q. Shi, X. S. Cheng, W. L. Chan, J. Song, *Biomed. Eng. Lett.* **2020**, *10*, 453; b) Y. Zhu, D. Joralmon, W. Shan, Y. Chen, J. Rong, H. Zhao, S. Xiao, X. Li, *Bio-Des. Manuf.* **2021**, *4*, 405; c) E. O. Bachtiar, O. Erol, M. Millrod, R. Tao, D. H. Gracias, L. H. Romer, S. H. Kang, *J. Mech. Behav. Biomed. Mater.* **2020**, *104*, 103649.
- [5] a) A. Jafari, Z. Ajji, A. Mousavi, S. Naghieh, S. A. Bencherif, H. Savoiji, *Adv. Mater. Technol.* **2022**, *7*, 2101636; b) V. Mishra, S. Negi, S. Kar, A. K. Sharma, Y. N. K. Rajbahadur, A. Kumar, *J. Thermoplast. Compos. Mater.* **2022**, *36*, 08927057221102857; c) A. S. Alagoz, V. Hasirci, *Emergent Mater.* **2020**, *3*, 429; d) U. Golcha, A. Praveen, D. B. Paul, *Direct Ink Writing of Ceramics for Bio Medical Applications—A Review*, IOP Conference Series: Materials Science and Engineering, Vol. 912, IOP, Bristol, UK **2020**, p. 032041.
- [6] a) S. Kyle, Z. M. Jessop, A. Al-Sabah, I. S. Whitaker, *Adv. Healthcare Mater.* **2017**, *6*, 1700264; b) G. Zhou, M.-C. Li, C. Liu, Q. Wu, C. Mei, *Adv. Funct. Mater.* **2022**, *32*, 2109593; c) M. Guvendiren, J. Molde, R. M. Soares, J. Kohn, *ACS Biomater. Sci. Eng.* **2016**, *2*, 1679.
- [7] a) S. Bom, R. Ribeiro, H. M. Ribeiro, C. Santos, J. Marto, *Int. J. Pharm.* **2022**, *615*, 121506; b) M. Elbadawi, T. Gustaffson, S. Gaisford, A. W. Basit, *Int. J. Pharm.* **2020**, *590*, 119868; c) T. C. R. Outrequin, C. Gamonpilas, W. Siriawatwechakul, P. Sreearunothai, *J. Food Eng.* **2022**, *342*, 111371.
- [8] a) H.-G. Yi, H. Kim, J. Kwon, Y.-J. Choi, J. Jang, D.-W. Cho, *Signal Transduction Targeted Ther.* **2021**, *6*, 177; b) M. D. A. Habib, B. Khoda, *J. Manuf. Processes* **2022**, *76*, 708.
- [9] a) S. J. Kim, G. Lee, J. E.-K. Park, *Adv. Mater. Technol.* **2022**, *7*, 2101326; b) D. Murata, K. Arai, K. Nakayama, *Adv. Healthcare Mater.* **2020**, *9*, 1901831; c) H. Taneja, S. M. Salodkar, A. Singh Parmar, S. Chaudhary, *J. Mol. Liq.* **2022**, *367*, 120390.
- [10] a) A. Mirek, H. Belaid, F. Barranger, M. Grzeczko, Y. Bouden, V. Cavallès, D. Lewinska, M. Bechelany, *J. Mater. Chem. B* **2022**, *10*, 8862; b) G. Bovone, E. A. Guzzi, S. Bernhard, T. Weber, D. Dranseikiene, M. W. Tibbitt, *Adv. Mater.* **2022**, *34*, 2106941.
- [11] a) T. J. Wallin, J. Pikul, R. F. Shepherd, *Nat. Rev. Mater.* **2018**, *3*, 84; b) A. Heiden, D. Preninger, L. Lehner, M. Baumgartner, M. Drack, E. Woritzka, D. Schiller, R. Gerstmayr, F. Hartmann, M. Kaltenbrunner, *Sci. Rob.* **2022**, *7*, eabk2119.
- [12] a) R. Yang, X. Chen, Y. Zheng, K. Chen, W. Zeng, X. Wu, *J. Mater. Chem. C* **2022**, *10*, 5380; b) K. Teng, Q. An, Y. Chen, Y. Zhang, Y. Zhao, *ACS Biomater. Sci. Eng.* **2021**, *7*, 1302.
- [13] a) A. I. Cernescu, A. I. Dinu, I. C. Stancu, A. Lungu, H. Iovu, *Biotechnol. Bioeng.* **2022**, *119*, 762; b) D. A. Foyt, M. D. A. Norman, T. T. L. Yu, E. Gentleman, *Adv. Healthcare Mater.* **2018**, *7*, 1700939.
- [14] a) M. K. Kim, W. Jeong, S. M. Lee, J. B. Kim, S. Jin, H.-W. Kang, *Biofabrication* **2020**, *12*, 025003; b) W. Wu, *Nano Lett.* **2020**, *15*, 964.
- [15] K. Dubbin, A. Tabet, S. C. Heilshorn, *Biofabrication* **2017**, *9*, 044102.
- [16] a) J. Hazur, R. Detsch, E. Karakaya, J. Kaschta, J. Teßmar, D. Schneiderreit, O. Friedrich, D. W. Schubert, A. R. Boccaccini, *Biofabrication* **2020**, *12*, 045004; b) S. Reakasame, A. R. Boccaccini, *Biomacromolecules* **2018**, *19*, 3.
- [17] a) J. Hauptstein, T. Böck, M. Bartolf-Kopp, L. Forster, P. Stahlhut, A. Nadernezhad, G. Blahetek, A. Zernecke-Madsen, R. Detsch, T. Jungst, J. Groll, J. Teßmar, T. Blunk, *Adv. Healthcare Mater.* **2020**, *9*, 2000737; b) J. Hauptstein, L. Forster, A. Nadernezhad, H. Horder, P. Stahlhut, J. Groll, T. Blunk, J. Teßmar, *Macromol. Biosci.* **2022**, *22*, 2100331.
- [18] a) B. G. Soliman, G. C. J. Lindberg, T. Jungst, G. J. Hooper, J. Groll, T. B. F. Woodfield, K. S. Lim, *Adv. Healthcare Mater.* **2020**, *9*, 1901544; b) S. Bertlein, G. Brown, K. S. Lim, T. Jungst, T. Boeck, T. Blunk, J. Tessmar, G. J. Hooper, T. B. F. Woodfield, J. Groll, *Adv. Mater.* **2017**, *29*, 1703404.
- [19] a) G. D. Bixler, B. Bhushan, *Philos. Trans. R. Soc., A* **2012**, *370*, 2381; b) D. C. Leslie, A. Waterhouse, J. B. Berthet, T. M. Valentin, A. L. Watters, A. Jain, P. Kim, B. D. Hatton, A. Nedder, K. Donovan, E. H. Super, C. Howell, C. P. Johnson, T. L. Vu, D. E. Bolgen, S. Rifai, A. R. Hansen, M. Aizenberg, M. Super, J. Aizenberg, D. E. Ingber, *Nat. Biotechnol.* **2014**, *32*, 1134.
- [20] G. Petrou, T. Cruzier, *Biomater. Sci.* **2018**, *6*, 2282.
- [21] a) M. A. Mcguckin, S. K. Lindén, P. Sutton, T. H. Florin, *Nat. Rev. Microbiol.* **2011**, *9*, 265; b) J. A. Voynow, B. K. Rubin, *Chest* **2009**, *135*, 505.
- [22] R. Bansil, B. S. Turner, *Curr. Opin. Colloid Interface Sci.* **2006**, *11*, 164.



- [23] O. Lieleg, C. Lieleg, J. Bloom, C. B. Buck, K. Ribbeck, *Biomacromolecules* **2012**, *13*, 1724.
- [24] T. Crouzier, K. Boettcher, A. R. Geonnotti, N. L. Kavanaugh, J. B. Hirsch, K. Ribbeck, O. Lieleg, *Adv. Mater. Interfaces* **2015**, *2*, 1500308.
- [25] J. P. Celli, B. S. Turner, N. H. Afdhal, R. H. Ewoldt, G. H. McKinley, R. Bansil, S. Erramilli, *Biomacromolecules* **2007**, *8*, 1580.
- [26] J. M. Coles, D. P. Chang, S. Zauscher, *Curr. Opin. Colloid Interface Sci.* **2010**, *15*, 406.
- [27] S. K. Linden, P. Sutton, N. G. Karlsson, V. Korolik, M. A. Mcguckin, *Mucosal Immunol.* **2008**, *1*, 183.
- [28] a) C. V. Duffy, L. David, T. Crouzier, *Acta Biomater.* **2015**, *20*, 51; b) C. Kimna, B. Winkeljann, J. Song, O. Lieleg, *Adv. Mater. Interfaces* **2020**, *7*, 2000735.
- [29] a) B. Winkeljann, M. G. Bauer, M. Marczynski, T. Rauh, S. A. Sieber, O. Lieleg, *Adv. Mater. Interfaces* **2020**, *7*, 1902069; b) L. Shi, R. Ardehali, K. D. Caldwell, P. Valint, *Colloids Surf., B* **2000**, *17*, 229; c) J. Song, T. M. Lutz, N. Lang, O. Lieleg, *Adv. Healthcare Mater.* **2021**, *10*, 2000831.
- [30] a) C. A. Rickert, I. Piller, F. Henkel, R. Fromme, O. Lieleg, *Biomater. Adv.* **2023**, *145*, 213233; b) C. A. Rickert, B. Wittmann, R. Fromme, O. Lieleg, *ACS Appl. Mater. Interfaces* **2020**, *12*, 28024; c) B. M. Naranjo, S. Naicker, O. Lieleg, *Adv. Mater. Interfaces* **2022**, *10*, 2201757.
- [31] a) J. S. Brand, L. Forster, T. Böck, P. Stahlhut, J. Teßmar, J. Groll, K. Albrecht, *Macromol. Biosci.* **2022**, *22*, 2100274; b) E. Olareă, B. A. Bălănuță, A. M. Onaș, J. Ghițman, H. Iovu, I.-C. Stancu, A. Serafim, *Polymers* **2021**, *13*, 1706.
- [32] M. Marczynski, K. Jiang, M. Blakeley, V. Srivastava, F. Vilaplana, T. Crouzier, O. Lieleg, *Biomacromolecules* **2021**, *22*, 1600.
- [33] I. Mironi-Harpaz, D. Y. Wang, S. Venkatraman, D. Seliktar, *Acta Biomater.* **2012**, *8*, 1838.
- [34] J. S. Brand, L. Forster, T. Böck, P. Stahlhut, J. Teßmar, J. Groll, K. Albrecht, *Macromol. Biosci.* **2021**, *22*, 2100274.
- [35] a) E. G. Crispim, J. F. Piai, I. T. Schüquel, A. F. Rubira, E. C. Muniz, *e-Polymers* **2006**, *6*, 062; b) T. Furukawa, H. Sato, R. Murakami, J. Zhang, Y.-X. Duan, I. Noda, S. Ochiai, Y. Ozaki, *Macromolecules* **2005**, *38*, 6445.
- [36] L. Ouyang, C. B. Highley, C. B. Rodell, W. Sun, J. A. Burdick, *ACS Biomater. Sci. Eng.* **2016**, *2*, 1743.
- [37] O. Lieleg, M. M. A. E. Claessens, Y. Luan, A. R. Bausch, *Phys. Rev. Lett.* **2008**, *101*, 108101.
- [38] a) A. Samani, J. Bishop, C. Luginbuhl, D. B. Plewes, *Phys. Med. Biol.* **2003**, *48*, 2183; b) V. Egorov, S. Tsyuryupa, S. Kanilo, M. Kogit, A. Sarvazyan, *Med. Eng. Phys.* **2008**, *30*, 206; c) A. Sarvazyan, *Handb. Elastic Prop. Solids, Liq., Gases* **2001**, *3*, 107.
- [39] F. Merino-Casallo, M. J. Gomez-Benito, S. Hervas-Raluy, J. M. Garcia-Aznar, *Cell Adhes. Migr.* **2022**, *16*, 25.
- [40] a) H. Tomás, C. S. Alves, J. Rodrigues, *Nanomed.: Nanotechnol., Biol. Med.* **2018**, *14*, 2407; b) M. Ghadiri, W. Chrzanowski, W. H. Lee, A. Fathi, F. Dehghani, R. Rohanzadeh, *Appl. Clay Sci.* **2013**, *85*, 64.
- [41] C. Kimna, M. G. Bauer, T. M. Lutz, S. Mansi, E. Akyuz, Z. Doganyigit, P. Karakol, P. Mela, O. Lieleg, *Adv. Funct. Mater.* **2022**, *32*, 2105721.
- [42] a) H. Yan, C. Seignez, M. Hjorth, B. Winkeljann, M. Blakeley, O. Lieleg, M. Phillipson, T. Crouzier, *Adv. Funct. Mater.* **2019**, *29*, 1902581; b) H. Yan, M. Hjorth, B. Winkeljann, I. Dobryden, O. Lieleg, T. Crouzier, *ACS Appl. Mater. Interfaces* **2020**, *12*, 19324.
- [43] S. Mohammadi, H. Ravanbakhsh, S. Taheri, G. Bao, L. Mongeau, *Adv. Healthcare Mater.* **2022**, *11*, 2102366.
- [44] L. E. Bostan, C. E. Clarkin, M. Mousa, P. R. Worsley, D. L. Bader, J. I. Dawson, N. D. Evans, *ACS Biomater. Sci. Eng.* **2021**, *7*, 2716.
- [45] M. Marczynski, C. A. Rickert, T. Fuhrmann, O. Lieleg, *Sep. Purif. Technol.* **2022**, *294*, 121209.
- [46] a) C. A. Rickert, M. G. Bauer, J. C. Hoffmeister, O. Lieleg, *Adv. Mater. Interfaces* **2022**, *9*, 2101716; b) C. A. Rickert, T. M. Lutz, M. Marczynski, O. Lieleg, *Macromol. Biosci.* **2020**, *20*, 2000090.
- [47] C. Nowald, A. Penk, H.-Y. I. Chiu, T. Bein, D. Huster, O. Lieleg, *Macromol. Biosci.* **2016**, *16*, 567.
- [48] M. Ghadiri, W. Chrzanowski, W. H. Lee, R. Rohanzadeh, *RSC Adv.* **2014**, *4*, 35332.